

Studies of Tetracene- and Pentacene-Based Organic Thin-Film Transistors Fabricated by the Neutral Cluster Beam Deposition Method

P. Syed Abthagir, Young-Geun Ha, Eun-Ah You, Seon-Hwa Jeong, Hoon-Seok Seo, and Jong-Ho Choi*

Department of Chemistry and Center for Electro- and Photo-Responsive Molecules, Korea University, Anam-Dong, Seoul 136-701, Korea

Received: August 30, 2005; In Final Form: October 13, 2005

The neutral cluster beam deposition (NCBD) method has been applied to produce and characterize organic thin-film transistors (OTFTs) based upon tetracene and pentacene molecules as active layers. Organic thin films were prepared by the NCBD method on hexamethyldisilazane (HMDS)-untreated and -pretreated silicon dioxide (SiO₂) substrates at room temperature. The surface morphology and structures for the tetracene and pentacene thin films were examined by atomic force microscopy (AFM) and X-ray diffraction (XRD). The measurements demonstrate that the weakly bound and highly directional neutral cluster beams are efficient in producing high-quality single-crystalline thin films with uniform, smooth surfaces and that SiO₂ surface treatment with HMDS enhances the crystallinity of the pentacene thin-film phase. Tetracene- and pentacene-based OTFTs with the top-contact structure showed typical source-drain current modulation behavior with different gate voltages. Device parameters such as hole carrier mobility, current on/off ratio, threshold voltage, and subthreshold slope have been derived from the current–voltage characteristics together with the effects of surface treatment with HMDS. In particular, the high field-effect room-temperature mobilities for the HMDS-untreated OTFTs are found to be comparable to the most widely reported values for the respective untreated tetracene and pentacene thin-film transistors. The device performance strongly correlates with the surface morphology, and the structural properties of the organic thin films are discussed.

1. Introduction

The recent progress made in organic thin-film-semiconductor devices has attracted much attention because of their promising applications in future electronic devices as flexible and economical alternatives to traditional silicon-based devices.^{1–6} Such applications may include organic thin-film transistors (OTFTs) for active matrix liquid crystal displays in which hydrogenated amorphous silicon (α -Si/H) devices have been used so far.⁷ Intensive studies have been carried out to improve OTFT characteristics, such as field-effect mobility, current on/off ratio, and long-term stability, through developing and optimizing small organic molecules or polymers. In recent years, the performance of some OTFTs stands in a state of competition with α -Si/H-based devices.^{8–13}

In organic molecule-based semiconductor devices, the molecules in the active layers stick together by virtue of relatively weak van der Waals interactions and maintain their individuality when they condense into solid thin-film crystals. Therefore, the spatial arrangement in the organic crystalline thin-film phase and the macroscopic properties of the material are primarily determined by the individual molecules, which is a unique characteristic of molecular engineering. This is exemplified by some fused-ring polycyclic aromatic hydrocarbons, such as the tetracene and pentacene shown in Figure 1 consisting of four and five aligned condensed benzene rings, respectively. In particular, the pentacene-based OTFTs have been extensively investigated up to now.^{1,14,15} The pentacene crystalline films with an ordered morphology have been generally obtained by

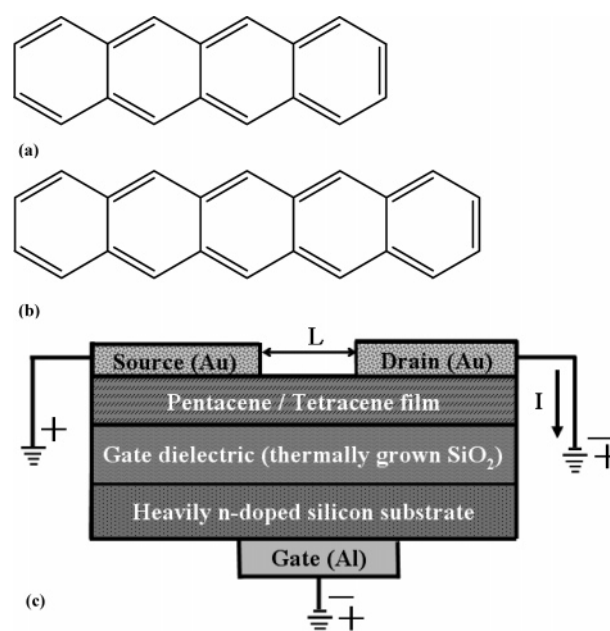


Figure 1. Molecular structures of (a) tetracene and (b) pentacene. (c) Schematic cross-sectional view of the OTFT with the top-contact structure and its bias condition.

vacuum evaporation, molecular beams, or pulsed laser deposition.^{16–20} In some device studies, a high charge-carrier mobility up to $\sim 3\text{--}5\text{ cm}^2/\text{V s}$, which is comparable to that observed in amorphous silicon, has been reported.^{12,14,21,22} Such a high mobility is attributed to the single crystallinity of the pentacene thin films that allows enhanced intermolecular carrier transport.

* To whom correspondence should be addressed. E-mail: jhc@korea.ac.kr. Fax: +82-2-3290-3121. Phone: +82-2-3290-3135.

In contrast, very few studies on tetracene-based OTFTs have been performed, and mobilities of $0.4 \text{ cm}^2/\text{V s}$ for the single-crystal device and $0.15 \text{ cm}^2/\text{V s}$ for the surface-pretreated tetracene thin-film device have been reported.^{23,24} Here, it should be noted that the above preparation of the organic single crystal phases is known to be reproducible only in very narrow ranges of the growth parameters, which are not easily achieved in the ordinary vapor deposition processes and/or the low-temperature processes on the plastic substrates.^{9,25}

The novel neutral cluster beam deposition (NCBD) method employed in this study is the less popular but promising deposition scheme.^{26–32} The method makes use of the cluster beam with the unique advantages of high directionality and translational kinetic energy when the organic vapor molecules undergo adiabatic expansion into a high vacuum. Because the neutral organic clusters consist of weakly bound molecules, the collision of the cluster beam with a substrate of interest such as SiO_2 induces the facile dissociation into individual molecules followed by active surface migration, resulting in the organic thin films with significant improvement in surface morphology, crystalline quality, packing density, and room-temperature substrate deposition. Such unique advantages cannot be achieved by conventional vapor deposition methods.

In this article, we present the fabrication and characterization of the tetracene- and pentacene-based OTFTs through the application of the NCBD method to deposit the organic active layers. First, we focus on the morphological and structural properties of the organic active layers deposited on the SiO_2 substrate at room temperature, together with an examination of the effects of surface treatment with the amphiphilic surfactant, hexamethyldisilazane (HMDS), as an ordered template. Afterward, the OTFTs with the top-contact structure in Figure 1 were fabricated, and the various device parameters, such as hole carrier mobility, current on/off ratio, threshold voltage, and subthreshold slope, were derived from the fits of the observed current–voltage characteristics of HMDS-untreated and -pretreated OTFTs. The device performance strongly correlates with the surface morphology, and the structural properties of the organic thin films are also discussed.

2. Experiment

The organic active layers of tetracene (Aldrich Co.) and pentacene (TCI Co.) were deposited on the substrate by the homemade NCBD apparatus. The system is presented in detail elsewhere,^{26–32} and only a relevant account is described here.

The NCBD chamber consists of the graphite crucible cell, the drift region, and the substrate. The deposition chamber was pumped by a 10 in. baffled diffusion pump, and the average base pressure was maintained below 1×10^{-6} Torr. The distance between the crucible cell and the substrate was 190 mm. The as-received organic active material was placed inside the enclosed cylindrical crucible cell with a 1.0-mm-diameter, 1.0-mm-long nozzle and sublimated by the resistive heating between 500 and 520 K for both tetracene and pentacene. The organic vapor molecules underwent adiabatic supersonic expansion into the high-vacuum drift region at a working pressure of $\sim 3 \times 10^{-5}$ Torr. The resultant highly directional, weakly bound neutral cluster beams were directly deposited onto the thermally grown 1000-Å-thick SiO_2 insulating layer on the heavily n-doped silicon substrates. Here, prior to beam deposition, the SiO_2 surface was pretreated with and without the amphiphilic hexamethyldisilazane (HMDS, Aldrich Co.) surfactant using the spin-coating method to examine the improvement in the crystalline quality of organic thin films and device performance.

In general, seven substrates were deposited simultaneously at room temperature. The growth rate was generally dominated by the temperature of the crucible cell and measured by a thickness monitor (Maxtek Inc.). The optimized deposition fluxes for tetracene and pentacene were determined at rates of 5 and 1 \AA/s , respectively.

The organic thin films without the HMDS surface treatment were compared with the HMDS-pretreated thin films. The characterization of the surface morphology and structures was performed by an alpha step surface profile monitor (Tencor Co.), atomic force microscopy (AFM: PSI Co.), and X-ray diffraction (XRD: Rigaku Co.). The XRD patterns were measured using $\text{Cu K}\alpha$ radiation with a wavelength of 0.1541 nm.

The tetracene- and pentacene-based OTFTs in this study employed the top-contact structure, and the cross section of the devices with bias conditions is shown in Figure 1c. A highly doped n-type silicon wafer coated with an aluminum layer was used as the gate electrode, and a 1000-Å-thick SiO_2 layer was thermally grown as the gate dielectric. Neutral cluster beams of tetracene and pentacene were deposited on the (HMDS-untreated and -pretreated) SiO_2 layer at room temperature. To form source and drain contacts, a 500-Å-thick gold layer was superimposed via e-beam evaporation through a proper rectangular-shaped shadow mask. For tetracene-based OTFTs, the channel had a width of $2000 \mu\text{m}$ and a length of $200 \mu\text{m}$, whereas for pentacene-based OTFTs the channel had a width of $1000 \mu\text{m}$ and a length of $200 \mu\text{m}$. The current–voltage characteristics of OTFTs were measured by an optical probe station connected with an HP4140B pA meter–dc voltage source unit. The drain-source current (I_{DS}) was monitored as a function of the drain-source voltage (V_{DS}) for various gate-source voltages (V_{GS}). Similarly, the drain-source current versus the gate-source voltage was measured at various drain-source voltages. Device parameters, such as hole carrier mobility, current on/off ratio, threshold voltage, and subthreshold slope, have been derived from the fits of the current–voltage characteristics for nearly 100 devices, together with an examination of the effects of surface treatment with HMDS on device performance.

3. Results and Discussion

3.1. Surface Morphology of Tetracene and Pentacene Thin Films. The characterization of surface morphology for the tetracene and pentacene thin films prepared by the NCBD method has been performed by recording AFM images. Figures 2 and 3 show the 2D micrographs for the organic thin films deposited on the HMDS-untreated and -pretreated SiO_2 substrates at room temperature. These films exhibit complete substrate coverage at a nominal thickness of 500 Å, which corresponds to a typical value for the active layers of OTFTs. The quantitative values of the root-mean-square roughness (R_{rms}) of the films were obtained by conducting section analyses over $5 \times 5 \mu\text{m}^2$ using the built-in software of the AFM apparatus.

In the case of tetracene deposition, both HMDS-untreated and -pretreated thin films in Figure 2a and b show the formation of grain crystallites with a granular structure. The grain size distribution and R_{rms} values for both films are measured to range from 0.28 to $0.40 \mu\text{m}$ in diameter and $\sim 40 \text{ \AA}$, respectively. In particular, the HMDS-untreated films are composed of more closely packed grain crystallites. Such quantitative values suggest that the weakly bound tetracene cluster beams undergo an effective fragmentation into active individual molecules, leading to smooth thin films consisting of submicrometer-sized crystallites on the SiO_2 substrate kept at room temperature. In

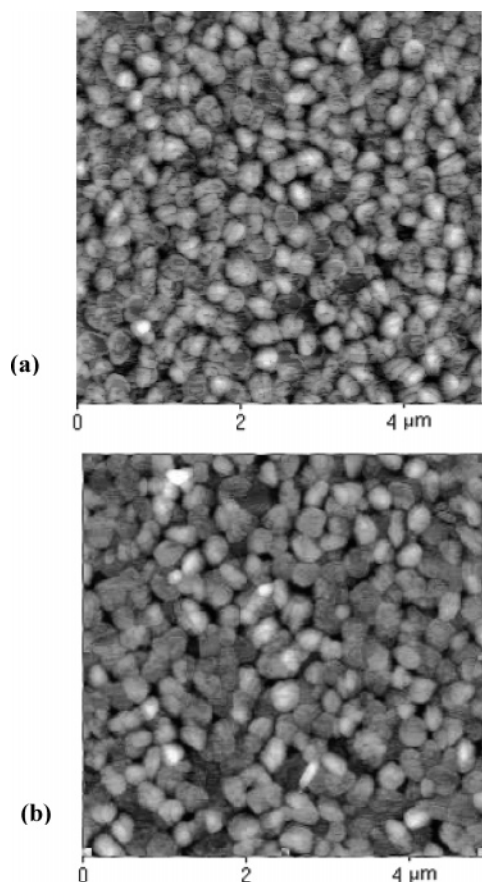


Figure 2. Two-dimensional micrographs for the 500-Å-thick tetracene thin films deposited on the (a) HMDS-untreated and (b) -pretreated SiO₂ substrates at room temperature (taken over $5 \times 5 \mu\text{m}^2$).

fact, the observed roughness in this study is much lower compared to the R_{rms} value ($\sim 100 \text{ \AA}$) recently reported for the vacuum-sublimed tetracene films produced at the same deposition rate of 5 \AA/s .²⁴ In addition, the surface treatment with the amphiphilic HMDS surfactant, which is closely correlated to the device performance, does not appear to favor the growth of tetracene films significantly at the tetracene/HMDS-pretreated SiO₂ interface. In the investigation of the SiO₂ substrate treatment with octadecyltrichlorosilane (OTS), no substantial improvement in the surface roughness of the tetracene films has been observed.²⁴ The effect of surface treatment on the crystallinity of the thin films is more clearly manifested in the XRD measurements to be discussed in the following section.

Figure 3 shows the AFM images of the HMDS-untreated and -pretreated pentacene thin films deposited at room temperature that are composed of grain crystallites with a dendritic structure. As in the tetracene films, a similar size distribution ranging from 0.25 to $0.38 \mu\text{m}$ is observed, whereas slightly higher R_{rms} values such as $\sim 50 \text{ \AA}$ for untreated films and $\sim 70 \text{ \AA}$ for HMDS-pretreated films are obtained. The HMDS-pretreated pentacene films consist of more closely packed grain crystallites, unlike the tetracene films. Such a high packing density suggests that during the initial accumulation at the pentacene/HMDS-pretreated SiO₂ interface the amphiphilic surfactant molecules capable of forming bonds with hydrophobic pentacene and hydrophilic SiO₂ simultaneously improve the packing between pentacene crystallites by reducing the lattice mismatch. The observed higher roughness might be attributed to the lower deposition rate of 1 \AA/s compared to that of tetracene, which is consistent with the general trend that the lower deposition flux increases both the film roughness and connectivity.²⁴ It should

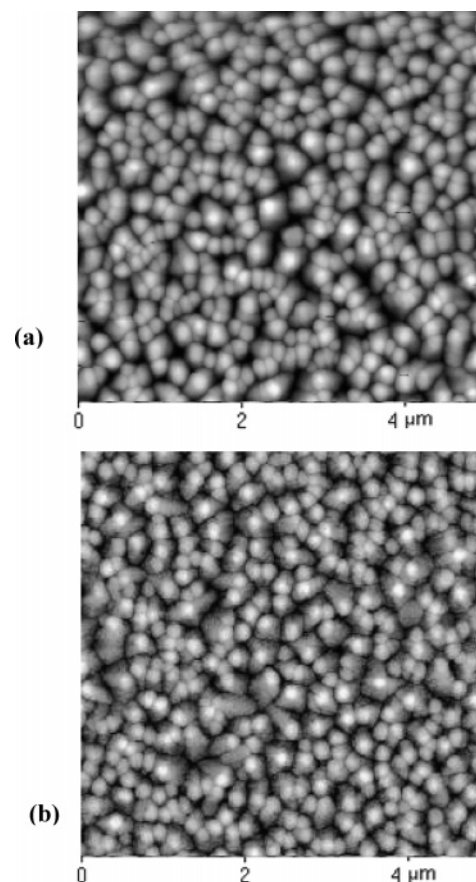


Figure 3. Two-dimensional micrographs for the 500-Å-thick pentacene thin films deposited on the (a) HMDS-untreated and (b) -pretreated SiO₂ substrates at room temperature (taken over $5 \times 5 \mu\text{m}^2$).

be noted that in comparison to the pentacene films reported in the literature, the formation of larger grain crystallite films with the smoother surface morphology again demonstrates the unique favorable characteristics achieved through the employment of the neutral cluster beams at high vacuum.^{33–35}

3.2. Structures of Tetracene and Pentacene Thin Films.

The characterization of the structures for the as-deposited tetracene and pentacene thin films has been conducted using the X-ray diffraction measurement operated with Cu K α radiation in a symmetric reflection, coupled θ – 2θ mode. Figures 4 and 5 exhibit the XRD results for the tetracene and pentacene thin films with an average thickness of 500 Å deposited on the HMDS-untreated and -pretreated SiO₂ substrates at room temperature. The strong, sharp first-order peaks as well as distinctive higher-order multiple peaks observed in the diffraction patterns demonstrate that these thin-film samples have highly ordered structures. Also, the effects of the HMDS surface treatment on the crystallinity of the films are clearly displayed.

As can be seen in Figure 4a and b, there are only three (00 l) reflections present with multiple d spacings in the HMDS-untreated and -pretreated tetracene thin films. The observed multiple peaks in the diffractograms can be fitted to a series of (00 l) reflection lines, and the interplanar spacing d_{001} from the peak positions is determined to be 12.5 \AA for both films. The spacing is in good agreement with the XRD investigation conducted by Akimichi et al.,³⁶ who reported $d_{001} = 12.1 \text{ \AA}$ for as-deposited tetracene films. Tetracene single crystals are found to have the triclinic structure with two molecules in the unit cell, and the observed vertical periodicity indicates the triclinic thin-film phase with the tetracene molecules oriented almost perpendicular to the substrate. In addition, the absence of any

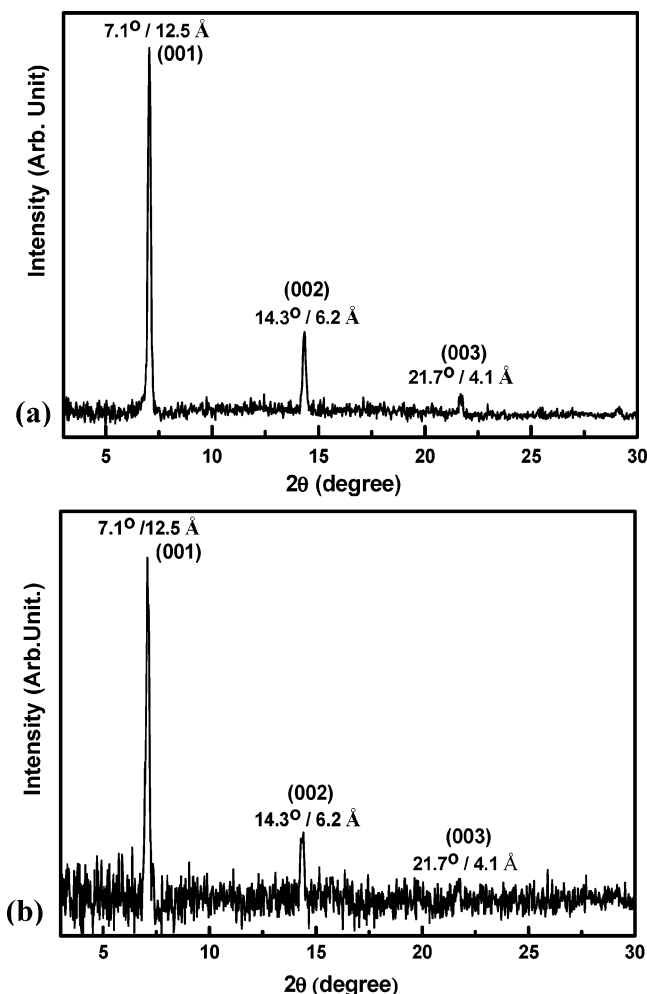


Figure 4. XRD patterns for the 500-Å-thick tetracene thin films deposited on the (a) HMDS-untreated and (b) -pretreated SiO_2 substrates at room temperature.

other (hkl) reflections implies that all of the crystals in the thin films are randomly oriented around the surface normal. The relatively poor signal-to-noise ratio in the XRD pattern of the HMDS-pretreated film in Figure 4b suggests that the amphiphilic surfactant treatment as an ordered template does not appear to affect the growth of tetracene films and the packing between tetracene crystallites substantially. The effect of the surfactant in the diffraction patterns is also consistent with the results shown in the AFM micrographs in the previous section.

In the case of the pentacene XRD patterns shown in Figure 5, more highly ordered pentacene films were obtained in comparison to tetracene thin films. In particular, the HMDS-pretreated thin film displayed very strong multiple peaks with an excellent signal-to-noise ratio, indicating that the surfactant treatment enhances the crystallinity significantly. The crystal structure of pentacene is also found to be triclinic, and the interplanar spacing d_{001} from the peak fitting to a series of (00 l) reflection lines is determined to be $d_{001} = 15.7 \text{ \AA}$. This suggests that the long axes of pentacene molecules are almost perpendicularly aligned to the surface to form a layered structure together with the random orientation of microcrystallites around the surface normal, as indicated by the absence of (hkl) reflections. Similar X-ray diffractograms have been reported by Minakata et al.,³⁷ who showed $d_{001} = 15.3 \text{ \AA}$. Here, it should be noted that the observed vertical periodicity in this study is attributed to the pentacene thin-film phase, not the single-crystalline bulk phase. The thin-film phase is a kinetically

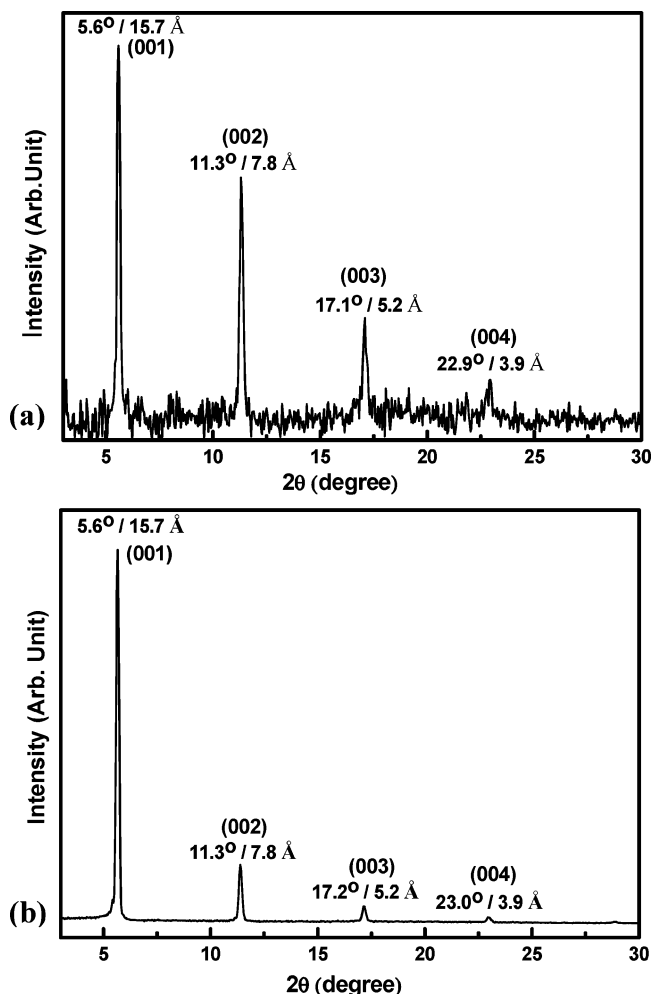


Figure 5. XRD patterns for the 500-Å-thick pentacene thin films deposited on the (a) HMDS-untreated and (b) -pretreated SiO_2 substrates at room temperature.

favored, substrate-induced metastable phase, whereas the bulk phase is a thermodynamically favored, stable single-crystalline phase.³⁴ With increasing film thickness, the pentacene is, in general, relaxed to the expected single-crystalline bulk phase. For the only 500-Å-thick pentacene films in Figure 5, the growth of the initial interface is strongly affected by the film–substrate interactions, which may also be very critical for the OTFT operation. In particular, the amphiphilic HMDS surfactant, because it is a well-ordered substrate, modifies the interface strongly, leading to the reduction of the lattice mismatch and the efficient formation of the observed pentacene thin-film phase. Even though it is not shown here, in the 5000-Å-thick film, which is 1 order of magnitude thicker than the thin films examined above, the coexistence of two phases was observed. However, the peaks corresponding to the single-crystalline bulk phase were found to be broadened, and the higher-order structures ($2\theta > 10^\circ$) were weaker, reflecting the increased disorder in the thicker single-crystalline films.

3.3. Characterization of Tetracene- and Pentacene-Based OTFTs. The tetracene- and pentacene-based OTFTs with the top-contact structure have been fabricated and characterized through the application of the NCBD method. The device structure and bias condition are shown in Figure 1c. The organic tetracene and pentacene films used in this study behave as p-type semiconductors. The performance of OTFTs was examined in the accumulation mode. The gate electrode was negatively biased with respect to the grounded source electrode, which

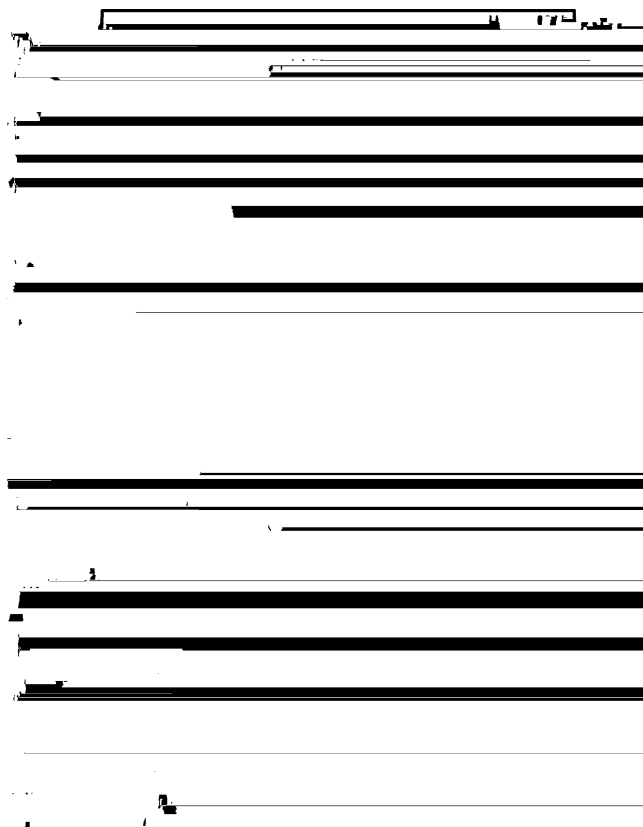


Figure 6. (a) Current–voltage characteristics for the HMDS-untreated tetracene-based OTFTs with a channel width of 2000 μm and a channel length of 200 μm . (b) Variation of $I_{\text{DS}}^{1/2}$ (left axis) and $\log(I_{\text{DS}})$ (right axis) vs V_{GS} at a constant drain-source voltage of $V_{\text{DS}} = -20$ V.

induced an accumulation of holes near the SiO_2 gate dielectric insulator–organic semiconductor interface. Typical plots of drain-source current (I_{DS}) as a function of the drain-source voltage (V_{DS}) for various gate-source voltages (V_{GS}) are displayed in Figures 6–9. The overall characteristics of OTFTs are adequately described by the standard field-effect transistor equations working in the accumulation mode. At a fixed V_{GS} , I_{DS} increases linearly with V_{DS} in the low- V_{DS} regime, and then I_{DS} tends to saturate in the high- V_{DS} regime because of the pinch off in the accumulation layer. In the saturation regime, I_{DS} increases with V_{GS} . From an analysis of the observed current–voltage characteristics, several device parameters, such as field-effect mobility (μ), current on/off ratio ($I_{\text{on}}/I_{\text{off}}$), threshold voltage (V_{T}), and subthreshold slope (S), can be derived.

Figures 6a and 7a show the current–voltage characteristics of the HMDS-untreated and -pretreated tetracene-based OTFTs with a channel width (W) of 2000 μm and a channel length (L) of 200 μm . In the saturation regime, I_{DS} can be expressed by the following relationship⁶

$$I_{\text{DS}} = \frac{WC_i\mu}{2L}(V_{\text{GS}} - V_{\text{T}})^2$$

where C_i is the capacitance per unit area of the gate dielectric insulator SiO_2 (for thermally grown 1000-Å-thick SiO_2 , $C_i = 34.5$ nF/cm²).³⁸ To obtain various device parameters, plots of $I_{\text{DS}}^{1/2}$ versus V_{GS} and $\log(I_{\text{DS}})$ versus V_{GS} were used. Figures 6b and 7b demonstrate the variation of $I_{\text{DS}}^{1/2}$ (left axis) and $\log(I_{\text{DS}})$ (right axis) versus V_{GS} at a constant drain-source voltage of $V_{\text{DS}} = -20$ V for both devices. μ and V_{T} were calculated from the slope and intercept, respectively, of the plot of $I_{\text{DS}}^{1/2}$

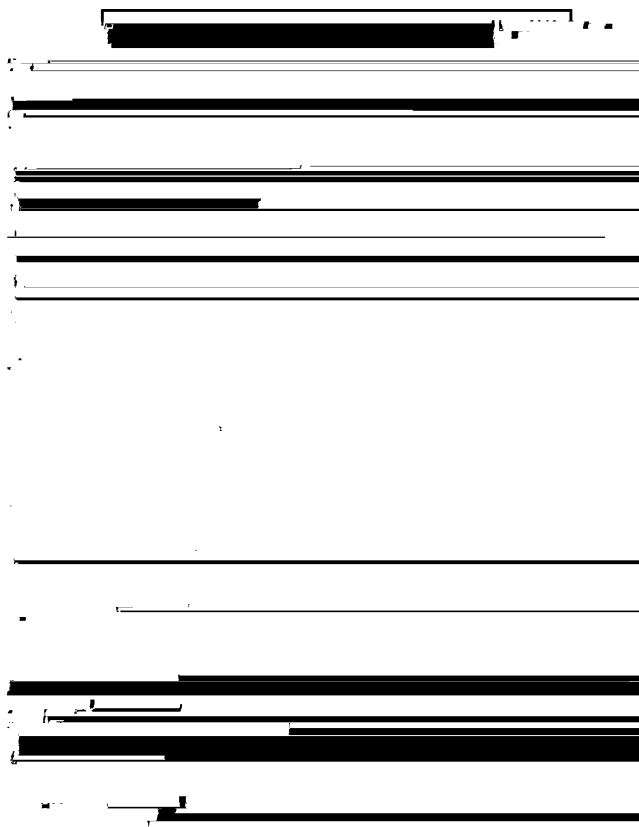


Figure 7. (a) Current–voltage characteristics for the HMDS-pretreated tetracene-based OTFTs with a channel width of 2000 μm and a channel length of 200 μm . (b) Variation of $I_{\text{DS}}^{1/2}$ (left axis) and $\log(I_{\text{DS}})$ (right axis) vs V_{GS} at a constant drain-source voltage of $V_{\text{DS}} = -20$ V.

versus V_{GS} , whereas the subthreshold slope defined by $S = \Delta V_{\text{GS}}/\Delta[\log(I_{\text{DS}})]$ was estimated from the slope of the plot of $\log(I_{\text{DS}})$ versus V_{GS} at $V_{\text{DS}} = -20$ V.³⁹

The various device parameters deduced from the OTFT characteristics are listed in Table 1. The tetracene-based OTFTs on HMDS-untreated gate dielectrics show $\mu = \sim 0.012$ cm²/V s, $I_{\text{on}}/I_{\text{off}} > 10^4$, $V_{\text{T}} = -4.5$ V, and $S = 3$ V/decade. In particular, the high field-effect mobility measured at room temperature is quite comparable to the best for the untreated tetracene thin-film transistors (0.01 cm²/V s at 15 °C) reported by Gundlach and co-workers.⁴⁰ Such good device performance is ascribed to the efficient charge-carrier transport in the intergrains composed of the tetracene crystallites formed by the neutral cluster beams. As manifested in the AFM images and the XRD diffractograms, the strong correlation between the surface morphology and the structural features of the submicrometer-sized crystallites with good film connectivity is directly reflected in the observed OTFT performance. For the HMDS-pretreated OTFTs, however, the surface treatment does not enhance the device performance significantly. The device shows $\mu = \sim 5.8 \times 10^{-3}$ cm²/V s, $I_{\text{on}}/I_{\text{off}} > 10^4$, $V_{\text{T}} = -3.0$ V, and $S = 2.5$ V/decade. This is in sharp contrast to the OTS-pretreated tetracene-based OTFTs, which show μ to be an order of magnitude larger than that of the untreated transistors.⁴⁰ This might be due to the poorer film packing between crystallites during the growth of tetracene films on the amphiphilic HMDS surfactant, as shown in the AFM image (Figure 2b), resulting in the less efficient intergrain hole transport. Such an observation is also consistent with the poorer signal-to-noise ratio obviously displayed in the XRD pattern of the HMDS-pretreated film in Figure 4b, confirming that one of the limiting factors determin-

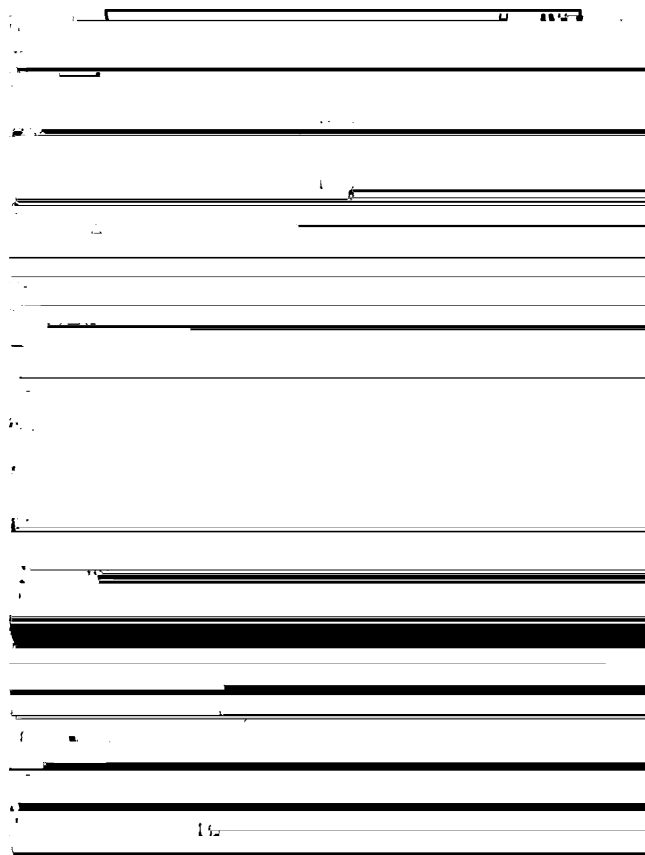


Figure 8. (a) Current–voltage characteristics for the HMDS-untreated pentacene-based OTFTs with a channel width of $1000\ \mu\text{m}$ and a channel length of $200\ \mu\text{m}$. (b) Variation of $I_{\text{DS}}^{1/2}$ (left axis) and $\log(I_{\text{DS}})$ (right axis) vs V_{GS} at a constant drain-source voltage of $V_{\text{DS}} = -25\ \text{V}$.

ing the field-effect mobility of OTFTs is the quality of the as-deposited crystalline thin films.

Figures 8a and 9a show the current–voltage characteristics of the HMDS-untreated and -pretreated pentacene-based OTFTs with a channel width of $1000\ \mu\text{m}$ and a channel length of $200\ \mu\text{m}$, respectively. Figures 8b and 9b demonstrate the variation of $I_{\text{DS}}^{1/2}$ (left axis) and $\log(I_{\text{DS}})$ (right axis) versus V_{GS} at a constant drain-source voltage of $V_{\text{DS}} = -25\ \text{V}$ for both devices. As tabulated in Table 1, the pentacene-based OTFTs show $\mu = \sim 0.19\ \text{cm}^2/\text{V}\ \text{s}$, $I_{\text{on}}/I_{\text{off}} > 10^5$, $V_{\text{T}} = -8.0\ \text{V}$, and $S = 1.8\ \text{V}/\text{decade}$ for HMDS-untreated gate dielectrics and $\mu = \sim 0.31\ \text{cm}^2/\text{V}\ \text{s}$, $I_{\text{on}}/I_{\text{off}} > 10^5$, $V_{\text{T}} = -7.5\ \text{V}$, and $S = 1.7\ \text{V}/\text{decade}$ for HMDS-pretreated gate dielectrics. The good overall device performance is mainly attributed to the growth of high-quality thin films deposited by the neutral cluster beams. In particular, the observed field-effect mobility belongs in the typically known range of $0.2\text{--}0.6\ \text{cm}^2/\text{V}\ \text{s}$ for the best thin-film pentacene-based transistors. Pentacene-based devices show μ to be 1 or 2 orders of magnitude larger than that of tetracene-based devices. This is due to the fact that pentacene exhibits a stronger tendency to form highly ordered thin films with good film connectivity, in

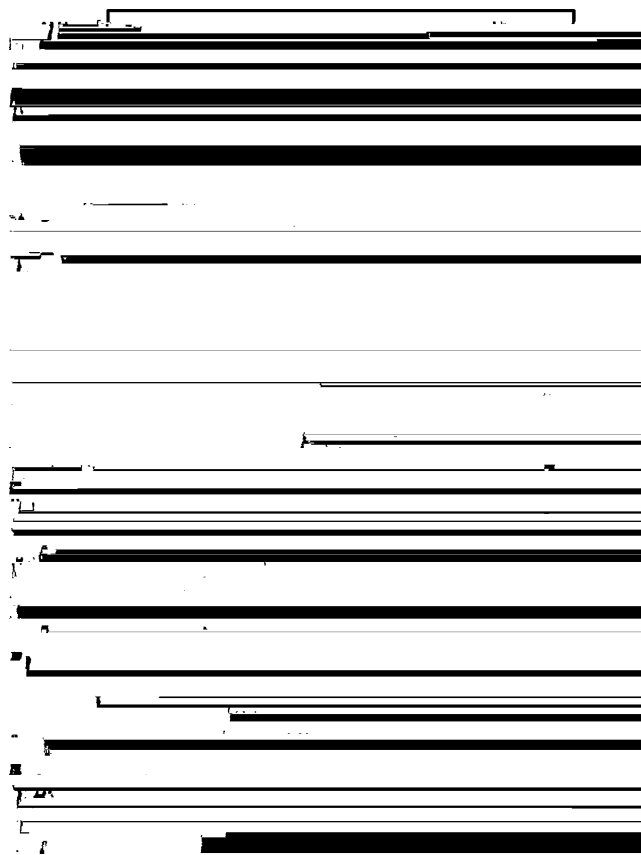


Figure 9. (a) Current–voltage characteristics for the HMDS-pretreated pentacene-based OTFTs with a channel width of $1000\ \mu\text{m}$ and a channel length of $200\ \mu\text{m}$. (b) Variation of $I_{\text{DS}}^{1/2}$ (left axis) and $\log(I_{\text{DS}})$ (right axis) vs V_{GS} at a constant drain-source voltage of $V_{\text{DS}} = -25\ \text{V}$.

which the maximum overlap of the π orbitals of adjacent pentacene molecules is induced, as displayed in the AFM images and the XRD diffractograms. Therefore, the more efficient hole transport in the pentacene thin films occurs through the intermolecular hopping mechanism. Another desirable device characteristic that is observed is the low subthreshold slope below about $1.8\ \text{V}/\text{decade}$, which is slightly higher than that reported for the α -Si/H-based transistors in the typical range of $0.3\text{--}1.5\ \text{V}/\text{decade}$. Such a low S is apparently dominated by the material properties of the pentacene films deposited by the NCBD method and is a significant enhancement because it is necessary to swing the OTFT gate voltage over a large range to obtain the low off current. In addition, unlike the tetracene cases, the surface treatment with HMDS improves the device performance. As shown in the XRD and AFM results described in the previous sections, it is clearly demonstrated that the higher mobility is quite strongly correlated with the improved surface morphology and structures of the pentacene films modified by the amphiphilic surfactant.

TABLE 1: Device Parameters Deduced from the OTFT Characteristics

	mobility μ ($\text{cm}^2/\text{V}\cdot\text{s}$)	on/off ratio	threshold voltage V_{T} (V)	subthreshold slope S (V/decade)	W/L ratio
tetracene without HMDS	$\sim 1.2 \times 10^{-2}$	10^4	-4.5	3	10
tetracene with HMDS	$\sim 5.8 \times 10^{-3}$	10^4	-3	2.5	10
pentacene without HMDS	~ 0.19	10^5	-8	1.8	5
pentacene with HMDS	~ 0.31	10^5	-7.5	1.7	5

4. Conclusions

The novel neutral cluster beam deposition method has been applied to prepare tetracene and pentacene thin films at room temperature. The surface morphology and structures examined by AFM and XRD demonstrate that the weakly bound and highly directional neutral cluster beams are quite efficient at producing high-quality single-crystalline thin films with the uniform, smooth surfaces and that the SiO₂ surface treatment with HMDS enhances the crystallinity of the pentacene thin-film phase. Tetracene- and pentacene-based OTFTs with the top-contact structure have been fabricated using the NCBD method. The device characteristics showed typical source-drain current modulation behavior with different gate voltages. Device parameters such as hole carrier mobility, current on/off ratio, threshold voltage, and subthreshold slope have been derived from the current–voltage characteristics together with the effects of surface treatment with HMDS. In particular, the high field-effect mobilities for the HMDS-untreated OTFTs measured at room temperature are found to be comparable to the most widely reported values for the respective untreated tetracene and pentacene thin-film transistors. The overall device characteristics are strongly correlated to the surface morphology and structures of the organic thin films.

Acknowledgment. We gratefully acknowledge the support of BK21 fellowships. This work was financially supported by NRL-KOSEF, MOST.

References and Notes

- (1) Ling, M. M.; Bao, Z. *Chem. Mater.* **2004**, *16*, 4824.
- (2) Reese, C.; Roberts, M.; Ling, M. M.; Bao, Z. *Mater. Today* **2004**, *7*, 20.
- (3) Horowitz, G. *Adv. Mater.* **1998**, *10*, 365.
- (4) Sheraw, C. D.; Nichols, J. A.; Gundlach, D. J.; Huang, J. R.; Kuo, C. C.; Klauk, H.; Jackson, T. N.; Kane, M. G.; Campi, J.; Cuomo, F. P.; Greening, B. K. *IEEE Int. Electron Devices Meet.* **2000**, 619.
- (5) Jackson, T. N. *IEEE Int. Semicond. Device Res. Symp.* **2001**, 340.
- (6) Dimitrakopoulos, C. D.; Malenfant, P. R. L. *Adv. Mater.* **2002**, *14*, 99.
- (7) Sheraw, C. D.; Zhou, L.; Huang, J. R.; Gundlach, D. J.; Jackson, T. N.; Kane, M. G.; Hill, I. G.; Hammond, M. S.; Campi, J.; Greening, B. K.; Franci, J.; West, J. *Appl. Phys. Lett.* **2002**, *80*, 1088.
- (8) Majewski, L. A.; Grell, M. *Synth. Met.* **2005**, *151*, 175.
- (9) Lim, S. C.; Kim, S. H.; Lee, J. H.; Yu, H. Y.; Park, Y.; Kim, D.; Zyung, T. *Mater. Sci. Eng., B* **2005**, *121*, 211.
- (10) Kang, G. W.; Park, K. M.; Song, J. H.; Lee, C. H.; Hwang, D. H. *Curr. Appl. Phys.* **2005**, *5*, 297.
- (11) Kelley, T. W.; Boardman, L. D.; Dunbar, T. D.; Muires, D. V.; Pellerite, M. J.; Smith, T. P. *J. Phys. Chem. B* **2003**, *107*, 5877.
- (12) Klauk, H.; Halik, M.; Zschieschang, U.; Schmid, G.; Radlik, W.; Weber, W. *J. Appl. Phys.* **2002**, *92*, 5259.
- (13) Choi, H. Y.; Kim, S. H.; Jang, J. *Adv. Mater.* **2004**, *16*, 732.
- (14) Kelley, T. W.; Baude, P. F.; Gerlach, C.; Ender, D. E.; Muires, D.; Haase, M. A.; Vogel, D. E.; Theiss, S. D. *Chem. Mater.* **2004**, *16*, 4413.
- (15) Sun, Y.; Liu, Y.; Zhu, D. *J. Mater. Chem.* **2005**, *15*, 53.
- (16) Lee, J. K.; Koo, J. M.; Lee, S. Y.; Choi, T. Y.; Joo, J.; Kim, J. Y.; Choi, J. H. *Opt. Mater. (Amsterdam, Neth.)* **2002**, *21*, 451.
- (17) Horowitz, G. *J. Mater. Chem.* **1999**, *9*, 2021.
- (18) Dinelli, F.; Murgia, M.; Biscarini, F.; De Leeuw, D. M. *Synth. Met.* **2004**, *146*, 373.
- (19) Yaginuma, S.; Yamaguchi, J.; Itaka, K.; Koinuma, H. *Thin Solid Films* **2005**, *486*, 218.
- (20) Itaka, K.; Hayakawa, T.; Yamaguchi, J.; Koinuma, J. *Appl. Phys. A* **2004**, *79*, 875.
- (21) Kelley, T. W.; Muires, D. V.; Baude, P. F.; Smith, T. P.; Jones, T. D. *Mater. Res. Soc. Symp. Proc.* **2003**, *771*, L6.5.
- (22) Gundlach, D. J.; Kuo, C. C.; Nelson, S. F.; Jackson, T. N. *IEEE 57th Annu. Device Res. Confer. Digest* **1999**, 164.
- (23) De Boer, R. W. I.; Klapwijk, T. M.; Morpurgo, A. F. *Appl. Phys. Lett.* **2003**, *83*, 4345.
- (24) Cicoira, F.; Santato, C.; Dinelli, F.; Murgia, M.; Loi, M. A.; Biscarini, F.; Zamboni, R.; Heremans, P.; Muccini, M. *Adv. Funct. Mater.* **2005**, *15*, 375.
- (25) Lee, J.; Hwang, D. K.; Choi, J. M.; Lee, K.; Kim, J. H.; Im, S.; Park, J. H.; Kim, E. *Appl. Phys. Lett.* **2005**, *87*, 023504.
- (26) Kim, J. Y.; Kim, E. S.; Choi, J. H. *J. Appl. Phys.* **2002**, *91*, 1944.
- (27) Ha, Y. G.; You, E. A.; Kim, B. J.; Choi, J. H. *Synth. Met.* **2005**, *153*, 205.
- (28) You, E. A.; Ha, Y. G.; Choi, J. H. *Synth. Met.* **2005**, *153*, 209.
- (29) Lim, H.; Kim, B. J.; Choi, J. H. *Synth. Met.* **2003**, *135–136*, 81.
- (30) Kim, J. Y.; Kim, E. S.; Choi, J. H. *Mater. Res. Soc. Symp. Proc.* **2001**, *667*, G3.12.
- (31) Kim, E. S.; Kim, K.; Jin, J. I.; Choi, J. H. *Synth. Met.* **2001**, *121*, 1677.
- (32) Kim, J. Y.; Kim, M.; Jeon, B. H.; Choi, J. H. *Synth. Met.* **2003**, *137*, 1023.
- (33) Song, C. K.; Jung, M. K.; Koo, B. W. *J. Korean Phys. Soc.* **2001**, *39*, S271.
- (34) Dimitrakopoulos, C. D.; Brown, A. R.; Pomp, A. *J. Appl. Phys.* **1996**, *80*, 2501.
- (35) Klauk, H.; Gundlach, D. J.; Nichols, J. A.; Jackson, T. N. *IEEE Trans. Electron Devices* **1999**, *46*, 1258.
- (36) Akimichi, H.; Inoshita, T.; Hotta, S.; Noge, H.; Sakaki, H. *Appl. Phys. Lett.* **1993**, *63*, 3158.
- (37) Minakata, T.; Imai, H.; Ozaki, M.; Saco, K. *J. Appl. Phys.* **1992**, *72*, 5220.
- (38) Santato, C.; Capelli, R.; Loi, M. A.; Murgia, M.; Cicoira, F.; Roy, V. A. L.; Stallinga, P.; Zamboni, R.; Rost, C.; Karg, S. F.; Muccini, M. *Synth. Met.* **2004**, *146*, 329.
- (39) Knipp, D.; Street, R. A.; Volkel, A.; Ho, J. *J. Appl. Phys.* **2003**, *93*, 347.
- (40) Gundlach, D. J.; Nichols, J. A.; Zhou, L.; Jackson, T. N. *Appl. Phys. Lett.* **2002**, *80*, 2925.